arXiv:astro-ph/0109457v1 25 Sep 2001

Simultaneous EUV and IR Observations of the Eclipsing Polar HU Aqr

Steve B. Howell

Astrophysics Group, Planetary Science Institute, Tucson, AZ 85705

howell@psi.edu

David R. Ciardi

Department of Astronomy, University of Florida, Gainesville, FL 32611

ciardi@astro.ufl.edu

Martin M. Sirk

Space Sciences Laboratory, UC Berkeley, CA 94720

sirk@ssl.berkeley.edu

Axel D. Schwope

Astrophysikalisches Institut Potsdam, An der Sternwarte 16, D-14482 Postdam, Germany

aschwope@aip.de

Received ______________________; accepted ______________________

Submitted to *AJ*

ABSTRACT

We present simultaneous EUV and infrared (J,K) observations of the polar HU Aqr obtained during August 1998 when the star was in a high mass accretion state. EUV and IR light curves and EUV spectra are presented and compared with previous observations. The accretion region on the white dwarf has increased in temperature (124,000K to 240,000K) and radius (0.04 R_{WD} to 0.06 R_{WD}) compared with previous EUV observations made during low mass accretion states. The EUV and IR photometric observations are shown to have a similar appearance as a function of orbital phase. The EUV photometry shows rapid changes and provides evidence for mass accretion via blobs. The high state IR light curves present an asymmetric double-humped shape with J=14.8 and K=14.1. We applied an ellipsoidal model fit to the observations and the result indicates that the cause of the modulated shape is both due to ellipsoidal variations from the Roche Lobe filling secondary star and a complex flux combination probably dominated at all orbital phases by cyclotron emission. The source of maximum cyclotron emission appears to be in the accretion column high above the white dwarf surface.

Subject headings: stars: individual (HU Aqr) — stars: magnetic fields — binaries: eclipsing — binaries: general — cataclysmic variables

1. Introduction

HU Aqr (RX J2107.9–0518) is a member of the polar or AM Her type of cataclysmic variable. Polars consist of an interacting pair of stars (white dwarf + red dwarf) in which the white dwarf primary is strongly magnetic. The material accreted from the low mass

secondary is magnetically controlled over the final portion of its flow being forced to funnel along the field lines and impact directly onto the white dwarf surface. The general location of the material impact site on the white dwarf surface is termed the accretion region. HU Aqr has an orbital period of 2.08 hr and the white dwarf magnetic field strength is estimated to be 36 MG.

High energy observations of polars provide us with direct information related to the accretion regions near the white dwarf surface surrounding the magnetic poles (See Sirk & Howell 1998; Schwope et al. 2001a). A number of high energy observations have been obtained for HU Aqr due to both its brightness at X-ray and EUV wavelengths and the fact that it is an eclipsing system. Eclipsing systems allow absolute orbital phase information to be obtained without ambiguity caused by accretion stream or accretion region eclipses. Phase dependent phenomena are then able to be referenced to an unchanging fiducial. A review of the observational history of HU Aqr, in particular the high energy observations, is provided by Schwope et al. (2001a).

Infrared observations of cataclysmic variables are useful as a tool to understand the secondary star which is typically of late spectral type and bright in the IR. These parameters are addressed through observations of ellipsoidal variations and the secondary star spectral energy distribution. IR observations also provide information about the cooler areas of the accretion stream and cyclotron radiation produced in the hot regions near the accretion spot. The usefulness of IR photometry is illustrated in Ciardi et al. (1998) and Howell et al. (2001) and IR spectroscopy in Howell et al. (2000).

In this paper, we present simultaneous EUV and infrared observations for HU Aqr obtained during a high mass accretion state in August 1998. The EUV observations allow us to measure the size and location of the accretion region and its temperature while IR photometry presents contributions from the accretion stream and coupling

region, the secondary star, and cyclotron radiation. The only previous attempt at such a multi-wavelength simultaneous approach was by Watson et al. (1989) using EXOSAT X-ray, optical, and IR data for the polar EF Eri. These authors concluded that the coincident dips seen in all the bands were caused by absorption in the accretion stream as it crosses the line of site to the accretion pole. Our new data allows a more detailed understanding of the process and we find that the two apparently distinct wavelength bands seem to have previously undiscovered commonalities as we find a correlation in their phase-resolved flux distributions.

2. Observations

2.1. *EUV* Observations

The *EUVE* satellite performed simultaneous spectroscopic and photometric observations in the EUV spectral range (Bowyer and Malina 1991) The principle instrument on board consists of a telescope which contains an imager and three separate spectrographs covering the range of 70 – 750Å. The bandpass of the deep survey (DS) imager is set by the Lexan/Boron filter, with a maximum transmission at 91 Å with a 90% bandpass of 67 – 178 Å. The imager allows for collection of photometric data simultaneously with the spectroscopic data. The *EUVE* obtains short wavelength (SW), medium wavelength (MW), and long wavelength (LW) data as three separately imaged dispersions covering the ranges of 70 – 170Å, 150 – 350Å, and 300 – 700Å respectively. All collected photons are position and time tagged providing high time-resolution and allowing the production of detailed light curves (e.g., Sirk and Howell 1998) and spectra (e.g., Craig et al. 1997; Mauche 1998; & Howell et al. 1997). Details of the photometric properties of the imaging telescopes on board the *EUVE* may be found in Sirk et al. (1997) and the spectroscopic instruments are reviewed in Abbott et al. (1996).

The *EUVE* observations of HU Aqr were obtained during the time period 1998 August 27 (21:47:10.0 GMT) to 1998 August 29 (21:30:49.0 GMT) with a total on-source integration time of 65.432 ksec. This time coverage contained 8.7 consecutive orbital periods of HU Aqr. During the *EUVE* observation, HU Aqr was detected with a mean count rate of 0.8 counts sec^{-1} photometrically and $\sim$0.1 counts sec^{-1} (near 100Å) spectroscopically. No EUV flux was detected long-ward of $\sim$110 Å due to absorption by the ISM. The high count rate observed made HU Aqr approximately 15 times brighter than any previous observation made with *EUVE* (see below) which spanned the time period of 1996-1997. The *EUVE* spectral data were extracted and reduced to phased-resolved 2-D images as described in the *EUVE* users manual, and then to 1-D spectra as discussed in Hurwitz et al. (1996). The photometric data reduction proceeded as described in Howell et al. (1995).

Figure 1 presents the mean EUV light curve obtained during the August 1998 observation binned in 15 sec intervals. Various phases of interest, which will be used later on, are identified on the figure and we note that the eclipse egress lasts less than 2 seconds. All data in this paper are phased on the ephemeris of Schwope et al. (1998),

$$T(HJD) = 2449217.345162(27) + 0.08682041520(82)N$$

with phase 0.0 representing the time of inferior conjunction of the secondary star. This ephemeris is equivalent to that of Schwope et al. (2001a) to within 10^{-4} seconds.

The previous observations of HU Aqr made with *EUVE* had too low of a count rate for useful spectra to be extracted. With the higher flux present in the current dataset, we are able to produce not only a summed spectrum covering the entire on-source time, but single spectra from phases of interest within the orbital cycle. Figure 2 shows our results for HU Aqr, labeled as to their phases as marked in Figure 1 and binned to a final spectral resolution of 0.8Å. The spectra shown in Figure 2 have been corrected for *EUVE* deadtime, primbsching, and the spectrograph effective area response function (See Abbott et al. 1996).

2.2. Infrared Observations

Using the 2.34 m infrared telescope at the Wyoming Infrared Observatory (WIRO) near Woods Landing, WY, HU Aqr was observed on UT 1998 August 29 & 30 in the near–infrared broadband filters J & K using the Aerospace Corporation 256 $\times$ 256 NICMOS3 camera. The camera has a spatial resolution of $0''.43$ per pixel for a total field of view of $110'' \times 110''$. The array has a quantum efficiency of $\gtrsim$ 60% over the $1 - 2$ μm wavelength range, an approximate dark current of $\lesssim 1$ e^-/second, and a readout noise of $\lesssim$ 30 electrons/pixel.

To minimize the effects of a variable sky background, the data were acquired in image "nod pairs." A nod pair consists of a "+beam" image and a "−beam" image which are spatially separated from each other by $20''$ in declination. The integration time of a single frame within a nod pair was 20 seconds. The image collection was performed such that a pair of images (one per "beam") was taken before changing filters. The images for the "nod pairs" are thus very close in time, $\sim$11 sec, which incorporates the readout and writing to disk of the first image and the slewing of the telescope by $20''$ (including settling time). The nod of the telescope was chosen carefully so that the source and two non–variable comparison stars remained within the field of view for both beams. After each filter–nod sequence, the filter was changed and the sequence repeated. Succesive filter pairs are separated by $\sim$2.5 minutes.

To increase the signal-to-noise ratio of the photometry, images within a "nod–pair" were registered and co-added, and standard differential photometry was performed on each co-added image as described in Howell, Mitchell, & Warnock (1988). Absolute photometry was obtained by observing a near–infrared standard star from the list of Elias et al. (1982) just prior to the start of the HU Aqr observations. The HU Aqr observations for the two nights were combined and phased on the orbital period using the same ephemeris as the

EUVE data. The final J and K light curves are shown in Figure 3 where they are compared with the 1996 J and K light curves from Ciardi et al. (1998). HU Aqr had mean J and K magnitudes of 16 and 15 respectively in 1996, while our new 1998 measurements have mean J and K magnitudes of 14.8 and 14.1 respectively.

3. Results

3.1. EUV

Figure 4 presents all the *EUVE* observations of HU Aqr. The August 1998 observation (bottom panel) has a much greater count rate than any of the other light curves in Fig. 4 and its shape has dramatically changed. The time sequence seen in Fig. 4 prior to the 1998 observation was originally thought to represent a progression of HU Aqr into a low mass accretion state. However, the 1998 observation would seem to indicate that *all* the previous *EUVE* observations were during a low mass accretion state, some just lower than others. Perhaps the most dramatic change observed in the 1998 EUV photometry of HU Aqr is the fact that the post-eclipse flux is now greater than the pre-eclipse flux, the opposite behavior to essentially all the low mass accretion state observations (Fig. 4). *ROSAT* observations of HU Aqr made in 1993 show similar count rate ratios compared with the August 1998 *EUVE* observation and also have higher post-eclipse fluxes (See Fig. 2 in Schwope et al. 2001a).

Many *EUVE* and *ROSAT* observations contain no flux from phase 0.9 to 0.97. The reason for this lack of flux is probably due to the accretion curtain blocking our view of the accretion region during this phase interval (See Sirk & Howell 1998; Schwope et al. 2001a). Additionally, we will see below that the flux level within the 0.9 to 0.97 phase window can be highly time variable.

Figure 5 presents the eight consecutive EUV HU Aqr light curves obtained during the

August 1998 observation. Each of the eight panels spans about a quarter day or 3 binary orbits of HU Aqr. The dotted line in Fig. 5 is the mean light curve of Fig. 1 illustrating that changes from orbit to orbit clearly exist. Note, for example, the change in flux near phase 0.925 related to effects in the far field accretion stream and the accretion curtain (near field stream) and the fast changes in absorption near phase 0.75 due to the near field accretion column. Sirk & Howell (1998) and Schwope et al. (2001a) show that changes in the shape of the soft X-ray/EUV light curves occur from observation to observation (months to years apart) and these changes provide evidence for the movement of the accretion stream due to changes in the mass accretion rate. Figure 5 provides evidence that rapid (few hour) changes occur during this high mass accretion state and are probably related to local opacity variations or blobs within the accretion stream and column (See §4).

Figure 6 shows our August 1998 spectrum during the bright phase (bottom panel) compared with the spectral sum of three previous observations (made during 1996) co-added over all phases with non-zero EUV flux. The final binned spectral resolution is 0.54Å for both plots in Fig. 6. While the older summed spectrum is of lower S/N, it is clear from its appearence that it is produced by a cooler accretion region than that in the August 1998 observations (see below).

3.2. Infrared

Infrared J and K light curves from 1998 and 1996 are shown in Figure 3. A comparison of the the light curves from the two epochs reveals some intriguing features. The most striking diffference between the light curves is the 1998 data are, on average, 2.5–3 times brighter than 1996 data. The infrared brightness increase is $\sim$15 times lower than the EUVE brightness increase.

At first glance the 1998 and the 1996 light curves appear to be similar in structure. Both sets of light curves display the deep stellar eclipse bottoming out at J$\sim$16.4 mag and K$\sim$15.4 mag. While the overall infrared brightness has increased between 1996 and 1998, the depth of the eclipse has not changed indicating that the infrared eclipses are total and the bottom of eclipse is representative of the back of the secondary star (See Ciardi et al. 1998).

In addition to the deep stellar eclipse, both J and K light curves are double-humped. The 1996 observations show two symmetric humps centered at orbital phases 0.25 and 0.75 which are well fit with an ellipsoidal variation model of the secondary stellar photosphere. The ellipsoidal model from Ciardi et al. (1998) is shown in Figure 3 and is overplotted upon the 1996 and 1998 data. The model, which explains the global variation of the 1996 data, does not explain the variations observed in the 1998 data. The 1998 "humps" are out of phase with those expected for ellipsoidal variations and are not symmetric in shape or amplitude. The ellipsoidal variations of the secondary star probably did not disappear between 1996 and 1998 (cf. Howell et al. 2000), but rather during this high accretion state, the secondary star flux is now over powered by orbitally modulated variations from another source. We note here a general warning to observers of polars that infrared light curves with "double–humped" structures do not necessarily consistute ellipsoidal variations of the secondary star. This same misconception has been seen in the optical as well (Howell et al. 2001). Thus, while ellipsoidal variations may still effect the light curve shape by providing some amount of the modulated structure, we will see below that the IR light curve in HU Aqr is quite complex and dominated by another source.

4. Discussion

4.1. EUV: Light Curves and Spectra

Sirk & Howell (1998) developed a three-dimensional model which allowed EUV photometric data to be fit in terms of various parameters dealing with the size, shape, and location of the accretion region on the white dwarf surface. Table 1 summarizes the findings from their original work on the 1996 *EUVE* observations of HU Aqr along with our new values determined from model fits to the current data. It has been assumed that the orbital period of HU Aqr has reminained constant and we have used the new determination of the system inclination, 85.6 degrees (Schwope et al. 2001a), instead of the value of 81 degrees available to Sirk & Howell. Schwope et al. (2001a) determined the size of the accretion region in HU Aqr for the high state 1993 *ROSAT PSPC* observations by analyzing eclipse ingress timings and by applying the 3-D Sirk and Howell model. In both cases, they found a consistant size of 0.052R_{WD} (1σ=0.02). This value is essentially the same as our high state determination listed in Table 1. In addition, there are enough photons to examine eclipse egress in the 1998 observations and its duration of 1.5-2.0 seconds, sets an upper limit on the EUV emitting region of 0.07 R_{WD}. Our Table 1 values for the 1996 and 1998 spot heights are the same but they are larger than the value of 0.014 R_{WD} given in Schwope et al. No uncertainty is given for the value of the height determined by these authors, but if it is similar to our uncertainty ($\pm$0.003), then we are not too far apart in our calculated heights. We find that the accretion region in HU Aqr has increased its area by a factor of $\sim$2.8, if approximately spherical in cross section, during this high mass accretion state. Uncertainties in the accretion region modeling procedures are fully discussed in Sirk & Howell (1998).

The three large dips seen in the EUV light curve (Fig. 1) are due to local absorption of EUV flux by the near field and far field accretion columns caused by our line of sight

through to the accretion region. Sirk & Howell (1998) found that a comparison of the EUV spectra obtained for UZ For, VV Pup, and AM Her during their broad dip phases with that observed during their bright phase (see their Figure 9) led to the result that spectra observed during the broad dips were softer than those obtained during the (assumed) unocculted bright phase. To see if this result holds for HU Aqr as well, we have taken the sum of our two HU Aqr "dip" spectra (Dip1 & Dip2; bottom two panels in Fig. 2) and compared them with the Bright phase spectrum. The low S/N in the dip spectrum made the comparison rather noisy but over the region of $70 - 90$Å, the spectrum appeared softer than that collected during the Bright phase, exactly what was found for UZ For, AM Her, and VV Pup.

Sirk and Howell (1998) have shown that the broad dip is caused by material very close to the accretion region (the near field stream) and modeled it with a cylindrically symmetric, uniformly dense absorber immediately above the accretion spot. Schwope et al. (2001a) show that it is not a cold absorber which is responsible for the broad dip. The broad dip in the EUV light curves of HU Aqr varies on short (binary period) time scales as can be seen in Figure 5. The large variations from orbit to orbit indicate that the broad dip is a changable feature in both phase and shape: the "broad dip" shape becoming manifest only when many individual orbits are averaged together. Warren, Sirk, & Vallerga (1995) found a similar behavior in the polar UZ For.

The many *ROSAT* and *EUVE* datasets for HU Aqr were used to search for correlations between accretion rate, spot latitude, stream dip phase, and broad dip phase as a function of time. The results are presented in Table 3 in Schwope et al (2001a). Most of the observations show the broad dip to occur at early orbital phases (ϕ = 0.69 to 0.77), however, a third of the observations show no clearly defined broad dip at all. To graphically illustrate the changes in the broad dip in HU Aqr, we show a normalized average EUV light

curve (dotted line) drawn on each of the individual light curves in Figure 4. This average curve was produced by taking every *EUVE* light curve of HU Aqr, normalizing each to its maximum value, averaging them all together, and then over-plotting them (scaled by each light curve maximum) on each single epoch light curve in Figure 4. Comparison of the "dipless" individual light curves in Figure 4 (May, July, & September 1996) with the normalized over-plotted average light curve reveals a deficit of flux at later phases (around $\phi = 1.0$ to 1.1). An extreme example of this effect can be seen in the *ROSAT* HRI April 1996 observation (Figure 2, Schwope et al. 2001a) where the second half of the light curve is nearly absent.

A quantitative correlation between the broad dip phase and the mass accretion rate is difficult to access but the following appears to be true. At a high accretion rate where we see the broad dip occur at an early phase, the low density portion of the ballistic stream latches onto the magnetic field first and strikes the WD at a relatively low longitude, and the higher density portion of the stream (blobs) penetrate further into the magnetic field and land on the WD at a greater longitude. Our view to the accretion spot through the column will then be most obscured at early phases (i.e., causing a flux deficit).

For the broad dip to occur at an early phase, it requires absorbing material to lead the EUV accretion spot in longitude on the white dwarf surface. When at later phases, the material must lag in longitude. We conclude that the near field accretion curtain is non-uniform in density at any given phase at any given time. Thus, at different times we are looking through varying amounts of absorbing material and these differences in column density are probably influenced by how the ballistic stream attaches on to the magnetic field lines within the coupling region. Even small mass accretion rate changes or blobby accretion will supply varying ram pressure causing the field lines to bend and changing the exact location of the coupling region for any given field line.

Mauche (1998) provided a detailed look at modeling the EUV spectra of polars. He concluded that absorbed blackbody models provide the best phenomenological description for the 70 − 180Å spectra of polars. However, Mauche and prior work by Paerels et al. (1994) both note problems with such a simple approach. The weak absorption edges and lines (mostly due to Ne species) are not properly dealt with and blackbody fits are unable to produce the observed EUV fluxes. Use of an irradiated solar composition stellar atmosphere model is likely to be more proper but models of this type need to be improved by adding in non-LTE effects, the underlying white dwarf, and absorption lines. Likewise, the quality of the spectral data to be modeled must greatly improve in order to allow quantitative analysis.

An additional complexity pointed out by Paerels et al. (1994) is the fact that a change in the fitted blackbody model continuum level will cause corresponding changes in the observed absorption line strengths. The use of simple blackbody models (especially to fit a mean spectrum) forces a "best fit continuum" criteria on the user, thereby fixing the apparent line strengths. Flucuations in intensity and spectral distribution which occur over time and orbitalphase are not accounted for. The S/N of the spectrum also plays a role here as it influences the selection of the best fit. A detailed example is given in Paerels et al. Given the moderate S/N of our HU Aqr spectra and the fact that an absorbed blackbody model does provide a decent fit to the observations, we opt to model our data in this manner. However, the reader should keep the above caveats in mind.

Using point sources (white dwarfs and B stars) observed with *EUVE* for the purpose of mapping out the ISM, we can estimate the interstellar column to HU Aqr. Ten sources in the *EUVE* data archive located in the direction of, and near the distance of HU Aqr (125 pc; Ciardi et al. 1998) were used to provide an initial estimate for the column density to HU Aqr of log N_H=19.75 (assuming HeI/H=0.1 and HeII/HeI=0.01). Starting with this

column density estimate and allowing our blackbody temperature and log N_H to be free parameters, we determined a best fit absorbed blackbody solution for our summed spectrum (bottom panel, Fig. 6). Our best fit yields a temperature of 240,000±40,000 Kelvins (20.68 kT (eV)) for the accretion region with a column to HU Aqr of log N_H=19.48±0.32. These values are in excellant agreement with those determined by Schwope et al. (2001a) for HU Aqr during a similar high mass accretion state *ROSAT-PSPC* observation made in October 1993. Attempts to fit absorbed blackbody models to the individual spectra from our August 1998 data or to the summed spectra from the 1996 datasets yielded large uncertainties due to their low counting statistics. The accretion region temperature for the 1996 low mass accretion state was found to be much cooler, with a best fit near ∼124,000 K, based on the spectral slope and assuming that the column density remained constant.

Spectral lines or line edges have been observed for a few polars in *EUVE* spectra (See a review by Mauche 1998). Mauche (1998) presents a detailed re-analysis of these same data and finds convincing evidence in a subset of the polars for lines due to Ne VI, VII, and VIII. Our August 1998 HU Aqr summed spectrum reveals a few features that may be real atomic absorption absorption lines and is of sufficient S/N to allow a qualitative examination of these possible spectral features. Searching the likely line species for polars present in the $70 - 100$Å range (N, O, Ne, Mg, and S), absorption lines due to Ne VIII at 73.5, 76(?), and 98.2 Å are the only set of consistant and possibly believable features. Ne VI line edges at 78.5 and 85.2 Å and that for O VI at 89.8 Å may be present. Ne VIII (98.2 Å) seems to be present in the 1996 low state spectrum as well.

The ionization potential for Ne VIII (239 eV) is too high to be provided by the EUV blackbody emission as the accretion region temperature (derived above) only provides $\bar{E} = \frac{3}{2}kT = 31$ eV. A temperature near 20 million Kelvins (20 keV) is necessary to begin to excite these Ne inner shell transitions. Thus, if we are to believe the Ne VIII spectral

features are real, we must invoke an additional heating source in the white dwarf atmosphere at or near the accretion region.

Ramsey et al. (1994) found that essentially all polar spectral energy distributions in the hard and soft (EUV) X-ray region are best fit by a two temperature model (an absorbed few 100,000K blackbody plus a harder thermal bremsstrahlung component). Typical shock temperatures (thermal bremsstrahlung fits) derived for X-ray observations of polars were found to be of order 15–30 keV, quite sufficient to produce Ne VIII. Schwope et al. (2001a) modeled HU Aqr with a bremsstrahlung component having a temperature of 20 keV, consistant with Ramsey et al. and sufficient to produce the neon lines. Thus for HU Aqr, Ne VIII absorption features superimposed on a blackbody spectrum would be consistant with a typical two-temperature model for the high energy emission from the accretion region in a polar. The existence of a harder component is believed to indicate that there is significant external heating of the white dwarf atmosphere by the bremsstrahlung radiation (an irradiated atmosphere) at and near the accretion region. The lack of any visible O VI lines in the HU Aqr spectrum suggests that the white dwarf atmosphere is heated only to small depths near the accretion region (van Teeseling et al. 1994 & See Fig. 1 in Paerels et al. 1996).

Polars are well known to show a "Soft X-ray Excess" (Ramsay et al. 1994; Warren and Mukai 1996), that is, the ratio L_{EUV}/L_{X-ray} is greater than the value of 0.55 predicted from theory (King and Watson 1987). Given that we have (non-simultaneous) EUV and X-ray observations of HU Aqr in both low and high states let us determine its soft X-ray excess during these times. From our 1998 high accretion state and 1996 low accretion state EUV observations we find L^{high}_{EUV}=1.16 × 10^{32} ergs sec^{-1} and L^{low}_{EUV}≃3.5 × 10^{31} ergs sec^{-1}. Using the X-ray flux observed during the similar 1993 high accretion state seen by *ROSAT* (Schwope et al. 2001b), we find L^{high}_{X-ray}=2.0 × 10^{31} ergs sec^{-1}. Low mass accretion states

(such as during 1996-97) have X-ray fluxes which are about 20 times lower overall than during a high state, thus $L^{low}_{X-ray} \simeq 1.0 \times 10^{30}$ ergs sec^{-1}. Schwope et al. (2001a) showed that during the accretion region eclipse, HU Aqr was detected with L_{X-ray}=2.2 $\times$ 10^{29} ergs sec^{-1} ($\sim$0.2 L^{low}_{X-ray}) apparently due to chromospheric activity on the secondary star. Using these determinations of the high energy luminosity of HU Aqr, we find $L^{high}_{EUV}/L^{high}_{X-ray}$=5.8 and $L^{low}_{EUV}/L^{low}_{X-ray} \geq 35$.

Both of our luminosity ratios are within the range determined for HU Aqr by Ramsay et al. (1994) of 3.1 (with a range of 1.5-33.4) during an apparent 1992 low mass accretion state (L_{X-ray}=1.9 $\times$ 10^{30} ergs sec^{-1}). While it appears that the soft X-ray excess in HU Aqr is greater during low mass accretion states, the range presented by Ramsay et al. is typical of what one finds within the uncertainties of model fitting with the low mass accretion states being of higher uncertainty due to their lower signal. If the deposition of mass blobs below the white dwarf surface is the cause of the soft X-ray excess as presently believed (See King 1995), our results may indicate that accretion by dense mass blobs during times of lower $\dot{M}$ occur in a larger proportion compared with accretion of lower density gas.

4.2. Infrared: Light Curves

It is reasonable to assume that the increase in infrared flux from 1996 to 1998 is directly related to the increased mass accretion state in HU Aqr as evidenced by the much brighter EUV flux. The EUV flux increase is both a result of the thermal increase and the size increase of the accretion region on the surface of the white dwarf (See Table 1). But where does the excess infrared emission emanate from? The three mostly likely sources are the thermal emission from the accretion region, cyclotron emission from the accretion region and column, and thermal emission from the accretion stream.

In Figure 7, the secondary star contribution to the infrared light curves has been subtracted away from the 1998 observations by scaling the ellipsoidal variation model from Ciardi et al. (1998) to the bottom of the stellar eclipse. The ellipsoidal subtracted infrared light curves still show modulations spanning nearly an order of magnitude and of a complex nature and no longer double-humped. Interestingly, the strongest excess infrared emission occurs when the accretion region is self-eclipsed by the white dwarf (region 7, Faint phase). This fact alone indicates that not all of the IR emission emanates from the accretion region located on the surface of the white dwarf, but rather a significant fraction must come from elsewhere.

The secondary star subtracted J & K fluxes (Fig. 7) and the EUV light curve (Fig. 1) are normalized to their maximum value and directly compared in Figure 8. Except for the infrared flux being non–zero during the EUV Faint Phase (region 7), the light curves are similar in morphology. In region 1 (Rise), there is a slight increase of infrared flux matching the EUV rise. The infrared rise is nearly twice as long in duration as the EUV rise probably a result of the infrared emission emanating from a region more extended than the EUV emitting region.

The overall decline of the EUV flux across regions 2–4 (the Dip phases) is matched in general by the infrared light curves. However, unlike the EUV, the general infrared flux decrease across the Dip phases is not a result of the accretion column passing in front of the emission region, but is likely the result of a change in the viewing angle of the beamed cyclotron emission (See Wickramasinghe & Ferrario 2000). Cyclotron emission is at its strongest when viewed at an angle of 90 degrees to the magnetic field lines which, depending on the exact orientation of the accretion column, corresponds to orbital phases of 0.6–0.7 in HU Aqr. It is only in the Stream Dip (region 4) and possibly in Broad Dip2 (region 3) that there is a corresponding dip in the infrared, and it only appears at J. The $< 1\%$ dip in J

is not as large as the EUV dip which is total ($> 4\%$), but it does imply that the accretion stream is more optically thick at J than at K.

The IR ingress during stellar eclipse (region 5) is similar in length to the ingress observed in the EUV but occurs slightly earlier in phase (See Schwope et al. 2001b). The infrared egress rises sharply with that of the EUV flux but the total recovery time is significantly longer than in the EUV. The difference in the infrared egress time is likely a result of viewing geometry and the larger IR emitting volume. As the secondary approaches inferior conjunction, the accretion column is viewed more and more straight-on. This orientation will also provide decreasing infrared cyclotron emission. Therefore, at the beginning of stellar eclipse, the projected area of the accretion column is relatively small and quickly eclipsed. But as the eclipse ends, the accretion column has rotated more perpendicular to the line of sight, increasing the time required to come fully out of eclipse. As the column rotates to a more perpendicular orientation with the viewing angle, the total IR emission increases as we see during the Faint (region 7) phase. This interpretation is slightly complicated by the fact that the level of (beamed) cyclotron emission from the accretion column is also dependent upon the line of sight viewing angle.

It would not be surprising if cyclotron emission dominates the infrared emission during the phases when the EUV accretion region is in view. However, can cyclotron emission contribute significantly during other phases, particularly the EUV Faint phase (region 7), or will the infrared emission be dominated by thermal emission from the coupling region and accretion stream? To test these ideas the J data was re-sampled at the K data rate. Because the J and K data were obtained in a sequence (K,J,K,J,...), for each K point the two adjacent J points in time were fit with a low order spline and the best-estimate J value was then interpolated for the exact time of each K data point. The intensity ratio of the J flux to the K flux was determined as a function of orbital phase and is shown in Figure 9.

Blackbody radiation, on the Rayleigh-Jeans tail, follows a λ^{-4} distribution which corresponds to a J/K flux ratio of ~ 11[1]. Cyclotron radiation, however, has a more complicated wavelength dependence. At long wavelengths, the "continuum" consists of optically thick emission which follows a Rayleigh-Jeans wavelength dependence. For magnetic field strengths typical of those in most polars, the optical and infrared spectral regions show the cyclotron continuum to be highly modulated by harmonic structures called cyclotron humps. The spectral dependence of cyclotron emission falls to a much shallower value (near $\lambda^{-1.5 \text{ to } -2.4}$) within the regions which are modulated by cyclotron humps with the slope becoming steeper as one moves to earlier harmonics.

Glenn et al. (1994) observed cyclotron harmonics 4, 5, and 6 in the optical spectrum of HU Aqr and fit them with a 10 keV plasma cyclotron model and a white dwarf magnetic field strength of 36 MG. These results have been confirmed by Schwope et al. (2001b). Thus, the first three cyclotron harmonics in HU Aqr will modulate the continuum in the J, H, and K bands as was pointed out by Ciardi et al. (1998). This interpretation is also consistent with model cyclotron spectra for a 10 keV plasma and B=35 MG calculated by Wickramasinghe & Ferrario (2000, See their Figure 32). Therefore, using a $\lambda^{-2.4}$ dependence for the IR cyclotron spectrum in HU Aqr, we would expect a J/K flux ratio of ~ 4.3 if the flux output is dominated by cyclotron emission.

Figure 9 reveals that the flux ratio ($F_{1.2\mu m}/F_{2.2\mu m}$) is generally flat throughout the orbit of the system, never climbing above $\sim$4.8 except during the stream dip and fall phases (regions 4 and 6). In the Faint phase (region 7) the ratio is almost exactly 4.3, making

[1]As a check on this value, we re-examined the J/K flux ratio for HU Aqr during the low mass accretion state reported on in Ciardi et al. (1998). During those observations, there was essentially no mass transfer and thus almost no cyclotron emission present. The J/K flux ratio was $\sim$10, the value expected for essentially pure blackbody emission.

the EUV faint phase infrared emission consistent with being essentially pure cyclotron emission. This is somewhat surprising given that the white dwarf has self-eclipsed the accretion region during these phases. However, during this high mass accretion state, the accretion column may extend far enough above the white dwarf surface such that significant cyclotron emission is visible even during the time when the accretion region is self-eclipsed. This is a surprising and unexpected hypothesis.

To see if such a tall accretion column may be possible, we calculate the shock height above the accretion region, that is, the approximate upper limit to where the 10 keV electron plasma would be confined. Using the mass estimate for the white dwarf, 0.6-7 $M_{\odot}$ (Schwope et al. 2001b), the mass accretion rate during an assumed similar high mass accretion state, $\dot{M} = 6 \times 10^{-11}$ $M_{\odot}$ yr^{-1} (Schwope et al. 2001a), and the expression for the shock height from Frank et al. (1992, Eq. 6.44), HU Aqr's shock will extend approximately 0.14 R_{WD} above the white dwarf surface. Geometric arguments show that if the shock height were at least 0.2 R_{WD} it would be visible to an observer even during the EUV Faint phase. Schwope et al. (2001b) examine the cyclotron radiation from HU Aqr in detail. They also propose that the cyclotron emission originates from a large height, higher than the soft X-ray emission, but only 0.03 R_{WD}. Fischer & Beuermann (2001) use 1-D hydrodynamic arguments to derive the location from which most of the cyclotron radiation emerges, i.e., the shock height. Applying their formulation to HU Aqr, the height of maximum cyclotron emission is calculated to be near 0.28 R_{WD}. This value is two times that determined from the simple equational form of Frank et al. given above, but is similar to the value needed herein to allow cyclotron radiation to be observed at all phases. Thus, given the uncertainties in the values used for these calculations, it seems plausible that significant cyclotron emission is observable throughout the orbit of HU Aqr during high mass accretion states.

The overall increase in the J/K flux ratio from phase 0.7 to phase 1.1, and its peak near phase 1.05, is likely a result of the *relative* increase of the thermal IR emission from the accretion region during the phases for which the observer has the most direct view. Additionally, during these phases the line of sight is increasingly straight onto the accretion column which decreases the strength of the (beamed) cyclotron emission. Thus, while the overall IR emission is *lower* in the phase interval 0.7–1.1 (see Figures 7 and 8), the relative contribution from thermal IR emission is *higher*, causing a rise in the J/K flux ratio. However, the ratio never approaches 11 as expected for pure blackbody emission, indicating that cyclotron emission remains dominate throughout the orbit.

5. Conclusion

We have presented simultaneous EUV and infrared high mass accretion state observations of the polar HU Aqr. The accretion region on the white dwarf shows an increase in temperature and radius by $\sim$2 times compared with results obtained during a low mass accretion state: the temperature increased from 124,000K to 240,000K and the radius from 2.2×10^7 cm to 3.7×10^7 cm. A two temperature model consisting of a hot thermal bremsstrahlung component and an absorbed blackbody component seems to fit the EUV observations. The EUV and IR photometric observations are shown to have a correlation with orbital phase although caused by distinct processes. HU Aqr had mean high state J and K magnitudes of 14.8 and 14.1 respectively. We have shown that the high mass accretion state IR light curve double-humped structure is *not* due to ellipsoidal variations from the secondary star but instead is caused by strong geometric modulation of the apparent size of the emitting region. Our results also show that during this high mass accretion state, the IR flux is dominated at all orbital phases by cyclotron emission emerging from high above the white dwarf surface, near 0.2 R_{WD}.

We wish to thank M. Huber for obtaining the IR photometry and K. Belle and C. Mauche for comments on a draft of this manuscript. An anonymous referee provided a number of useful comments leading to improvements in the presentation. The research was supported by an AO-7 EUVE mini-grant and NASA grant NAG5-8644 to SBH and an AO-6 EUVE mini-grant to CRD. This work was supported in part by the German DLR under grant 50 OR 9706 8.

REFERENCES

Abbott, M., et al. 1996, ApJ Suppl., 107, 451

Bowyer, S., & Malina, R., 1991, in "Extreme Ultraviolet Astronomy", ed. R. Malina and S. Bowyer, (New York: Pergammon Press), 397

Ciardi, D., Howell, S. B., Hauschildt, P., and Allard, F., 1998, ApJ, 504, 450.

Cropper, M., 1990, Space Science Reviews, 54, 195.

Craig, N., et al. 1997, ApJ Suppl., 113, 131.

Elias, J. H. et al. 1982, AJ, 87, 1824

Fischer, A., & Beuermann, K., 2001, A&A, 373, 211.

Frank, J., King, A., & Raine, D., 1992, *Accretion Power in Astrophysics*, Cambridge University Press, New York.

Glenn, J., Howell, S. S., Schmidt, G., Liebert, J., Grauer, A., & Wagner, R. M., 1994, ApJ., 424, 967.

Howell, S. B., Gelino, D., & Harrison, T., 2001, AJ, 121, 482.

Howell, S. B., Ciardi, D., Dhillon, V., & Skidmore, W., 2000, ApJ, 530, 904.

Howell, S. B., Sirk, M., Malina, R. F., Mittaz, J. P. D., & Mason, K. O., 1995, ApJ, 439, 991

Howell, S. B., Sirk, M., Ramsey, G., Cropper, M., Potter, S., & Rosen, S., 1997, ApJ, 485, 333

Howell, S. B., Mitchell, K. J., & Warnock, A. 1988, AJ, 95, 247

Hurwitz, M., Sirk, M., Bowyer, S., & Ko, Y., 1997, ApJ 477, 390

King, A., 1995, in "Cape Workshop on Magnetic Cataclysmic Variables", eds. D. Buckley & B. Warner, ASP Conf. Series Vol. 85, p. 21

King, A., & Watson, M., 1987, MNRAS, 227, 205

Mauche, C., 1998, in “Annapolis Workshop on Magnetic Cataclysmic Variables”, eds. C. Hellier & K. Mukai, ASP Conf. Series Vol. 157, p. 157

Paerels, F., Heise, J., & van Teeseling, A., 1994, ApJ, 426, 313

Paerels, F., Hur, M., Mauche, C., & Heise, J., 1996, ApJ, 464, 884

Ramsey, G., Mason, K., Cropper, M., Watson, M., & Clayton, K., 1994, MNRAS, 270, 692

Schwope, A., et al. 1998, in “Wild Stars in the Old West”, eds. S. B. Howell, E. Kuulkers, & C. Woodward, ASP Conf. Series Vol. 137, p. 44

Schwope, A., Schwarz, R., Sirk, M., & Howell, S. B., 2001a, A&A, 375, 419

Schwope, A., Thomas, H.-C., Mantel, K.-H., & Haefner, R., 2001b, A&A, submitted.

Sirk, M., et al. 1997, ApJ Suppl., 110, 347

Sirk, M., & Howell, S. B., 1998, ApJ, 506, 824

van Teeseling, A., Heise, J., & Paerels, F., 1994, A&A, 281, 119

Warren, J., Sirk, M., & Vallerga, J., 1995, ApJ, 445, 909.

Warren, J., & Mukai, K., 1996, in “Astrophysics in the Extreme Ultraviolet”, eds. S. Bowyer & R. Malina, Kluwer Publishers, p. 325

Watson, M., King, A., Jones, D., & Motch, C., 1989, MNRAS, 237, 299.

Wickramasinghe D., & Ferrario, L., 2000, PASP, 112, 873

Figure captions

Figure 1: August 1998 EUV light curve for HU Aqr. Various phases of interest are marked on the plot.

Figure 2: Phase-resolved EUV spectra for HU Aqr. The four panels show (top to bottom) the total summed dataset, the Bright phase, the Dip1 phase, and the Dip2 phase. The 1σ error is given for each panel and the final binned spectral resolution is 0.8Å. See Figure 1 for the phase intervals involved.

Figure 3: Orbitally phased J (top) and K (bottom) photometry of HU Aqr are plotted for the 1996 data (crosses) and the 1998 data (circles). The solid black curve is the ellipsoidal model for the secondary star from Ciardi et al. (1998) and has been overlayed upon both the 1996 and 1998 data. Estimated 1σ uncertainties in both J and K are ±0.2 mag. Note the good agreement of the depth of the eclipse in the 1996 and 1998 observations and how well the ellipsoidal model fits the 1996 observations.

Figure 4: Historical retrospective of previous *EUVE* observations of HU Aqr and the August 1998 high accretion state light curve (bottom panel). Note the y-axis scale change for the August 1998 observation. The dotted line is the global average *EUVE* light curve, scaled in each panel to the maximum value. See text for details.

Figure 5: Eight consecutive binary orbits of HU Aqr from the 1998 *EUVE* observation. Each light curve consists of ∼7400 seconds of data (∼1 binary orbit) composed of four consecutive EUVE satellite orbits and phased on the binary ephemeris. The data are summed in 20 sec bins. The top of each plot gives the start time for each light curve. Note the rapid changes that occur in each 2 hour time interval, especially near phases 0.7–0.9.

Figure 6: Summed spectrum for HU Aqr during low mass accretion states (1996, top) and a our high mass accretion spectrum (1998, bottom). The spectra are best fit with an absorbed blackbody model yielding temperatures of ∼124,000 K and 240,000 K respectively. The

Table 1. Accretion Region Parameters for HU Aqr

Parameter[a]	May 1996[b]	August 1998[c]
Spot Radius (R_{WD})	0.036	0.061(5)
Spot Radius (10^7 cm)	2.16	3.66
Spot Area (10^{15} cm^2)	1.47	4.21
Fractional Emitting Area	3.27×10^{-4}	9.36×10^{-4}
Spot Height (R_{WD})	0.021	0.023(3)
Spot Latitude (degrees)	34.5[d]	36(7)
Spot Longitude (degrees)	49	49(1)
Accretion Region Temperature (K)	$\sim$124,000	240,000(40,000)

[a]We assume here a white dwarf radius of 6000 km (Ciardi et al. 1998).

[b]Sirk & Howell (1998)

[c]Numbers in () are 1σ errors.

[d]This value was reported as 40 degrees in Sirk & Howell (1988), but using the new binary inclination estimate of 85.6 degrees (Schwope et al. 2001a), compared with the older value of 81, we subtract 4.6 degrees from the Sirk & Howell value.

dotted line indicates the 1σ uncertainty in the flux, the locations of expected and likely features are marked, and the final binned spectral resolution is 0.54Å.

Figure 7: Plot of the phased 1998 J and K flux densities ($F_{1.2\mu m}$ and $F_{2.2\mu m}$) after the subtraction of the secondary star mean level and ellipsoidal variations based on the model in Ciardi et al. (1998). The vertical lines and numbers indicate the divisions labeled and named in Figure 1. The regions marked will be used again in Figures 8 & 9.

Figure 8: Plot of the infrared and EUV flux densities. Each dataset has been normalized such that the maximum point in each light curve is unity and the EUV data has been re-sampled to match the J and K points respectively. The vertical lines and numbers indicate the divisions labeled and named in Figure 1.

Figure 9: The J ($F_{1.2\mu m}$) and K ($F_{2.2\mu m}$) flux densities (as in Figure 7) have been directly ratioed and plotted as a function of orbital phase. The estimated uncertainty in the flux ratio is $1\sigma = \pm 0.35$. The stellar eclipse points (region 5) have been omitted from this figure and the J data have been re-sampled at the K data rate. The solid histogram is the EUV flux scaled such that the maximum EUV point matches the maximum J/K flux ratio. A $F_{1.2\mu m}/F_{2.2\mu m}$ ratio of 4.3 indicates that the IR emission is dominated by cyclotron radiation. See text for details.

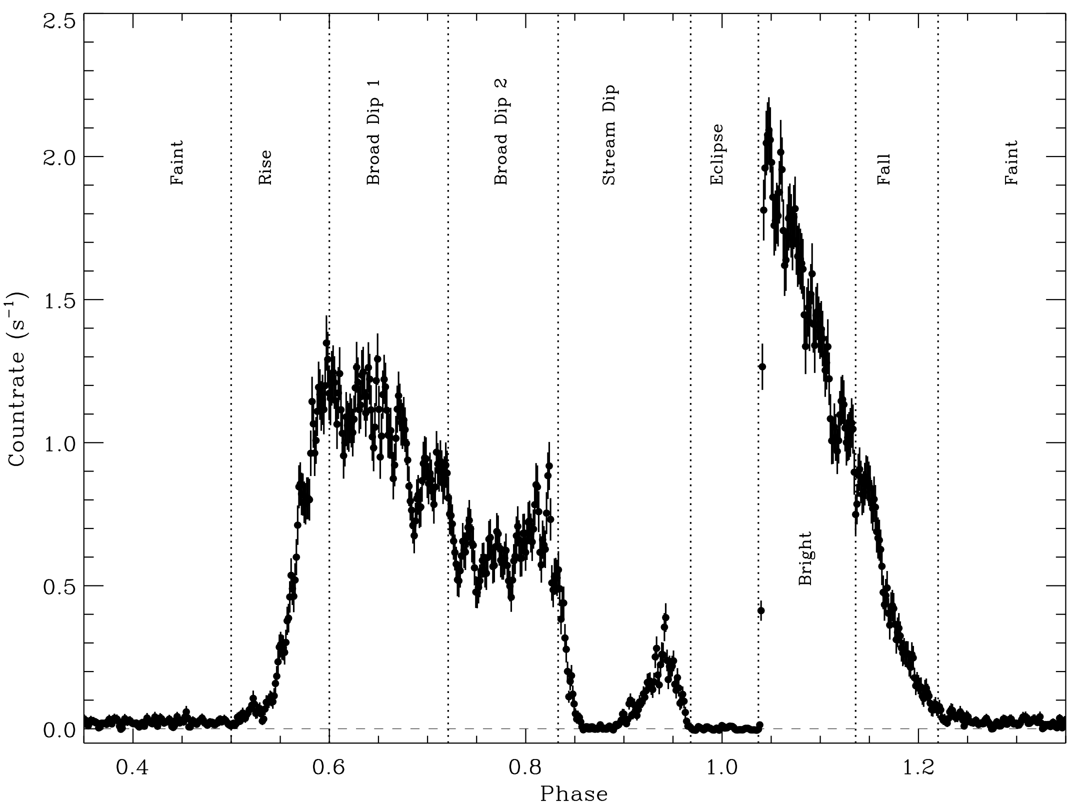
2.5
2.0
1.5
1.0
0.5
0.0
Countrate (s^{-1})
0.4
0.6
0.8
1.0
1.2
Phase
Faint
Rise
Broad Dip 1
Broad Dip 2
Stream Dip
Eclipse
Bright
Fall
Faint

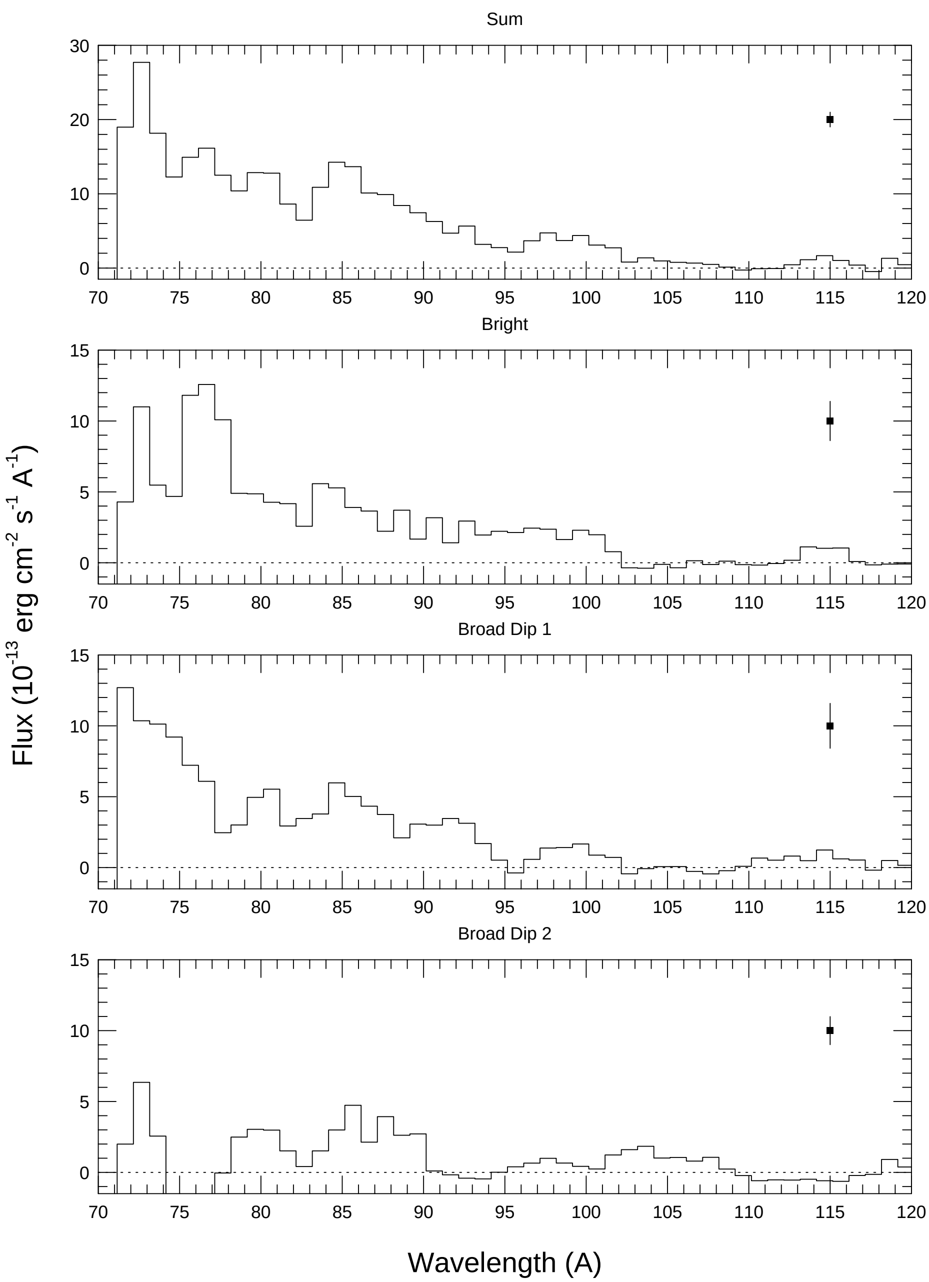
Sum
Bright
Broad Dip 1
Broad Dip 2
Flux (10^{-13} erg cm^{-2} s^{-1} A^{-1})
Wavelength (A)
70
75
80
85
90
95
100
105
110
115
120
0
10
20
30
5
15

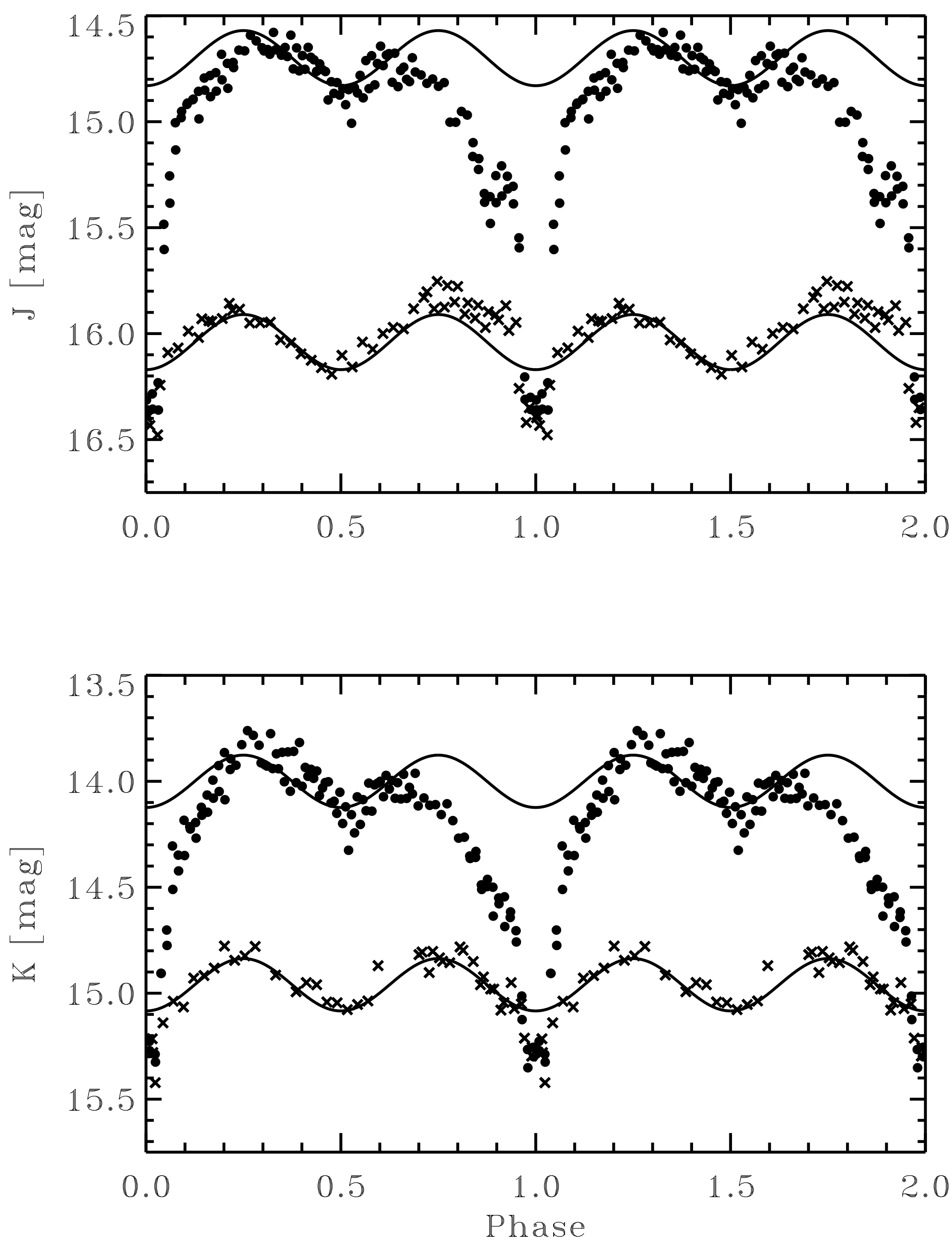
14.5
15.0
15.5
16.0
16.5
J [mag]
0.0
0.5
1.0
1.5
2.0
13.5
14.0
14.5
15.0
15.5
K [mag]
0.0
0.5
1.0
1.5
2.0
Phase

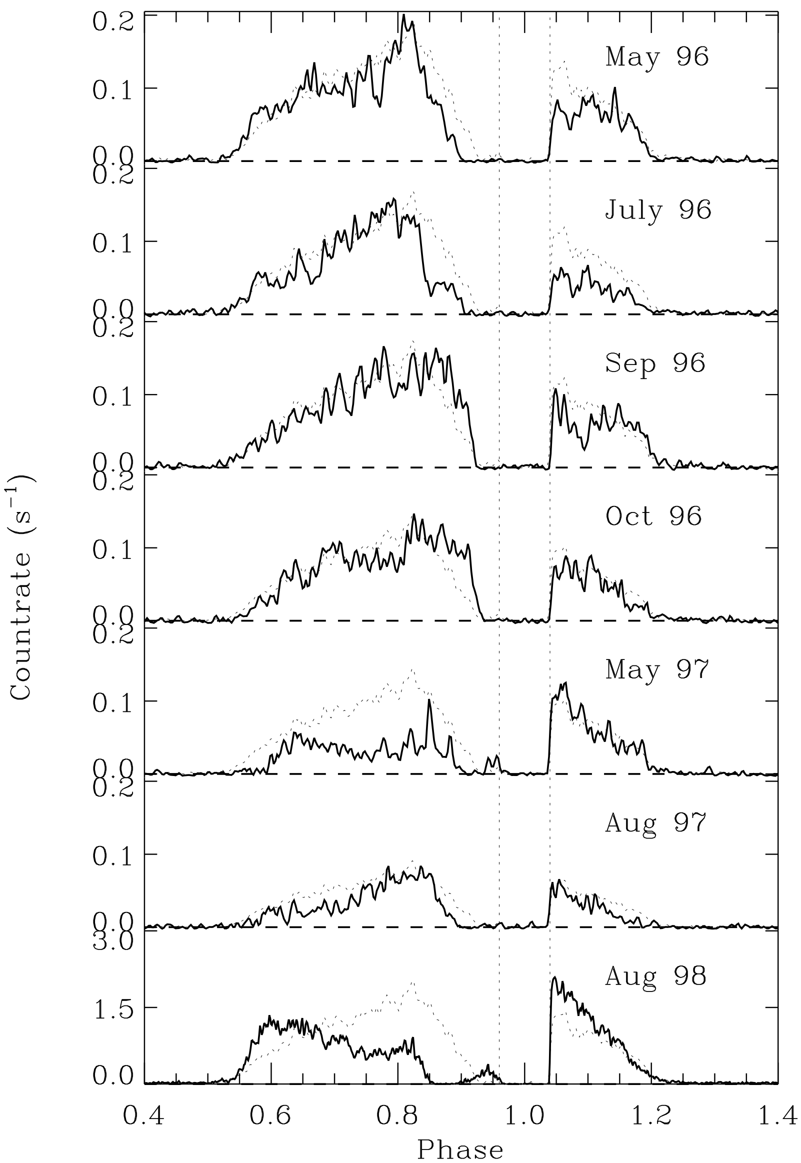

May 96
July 96
Sep 96
Oct 96
May 97
Aug 97
Aug 98
Countrate (s^{-1})
Phase
0.0
0.1
0.2
1.5
3.0
0.4
0.6
0.8
1.0
1.2
1.4

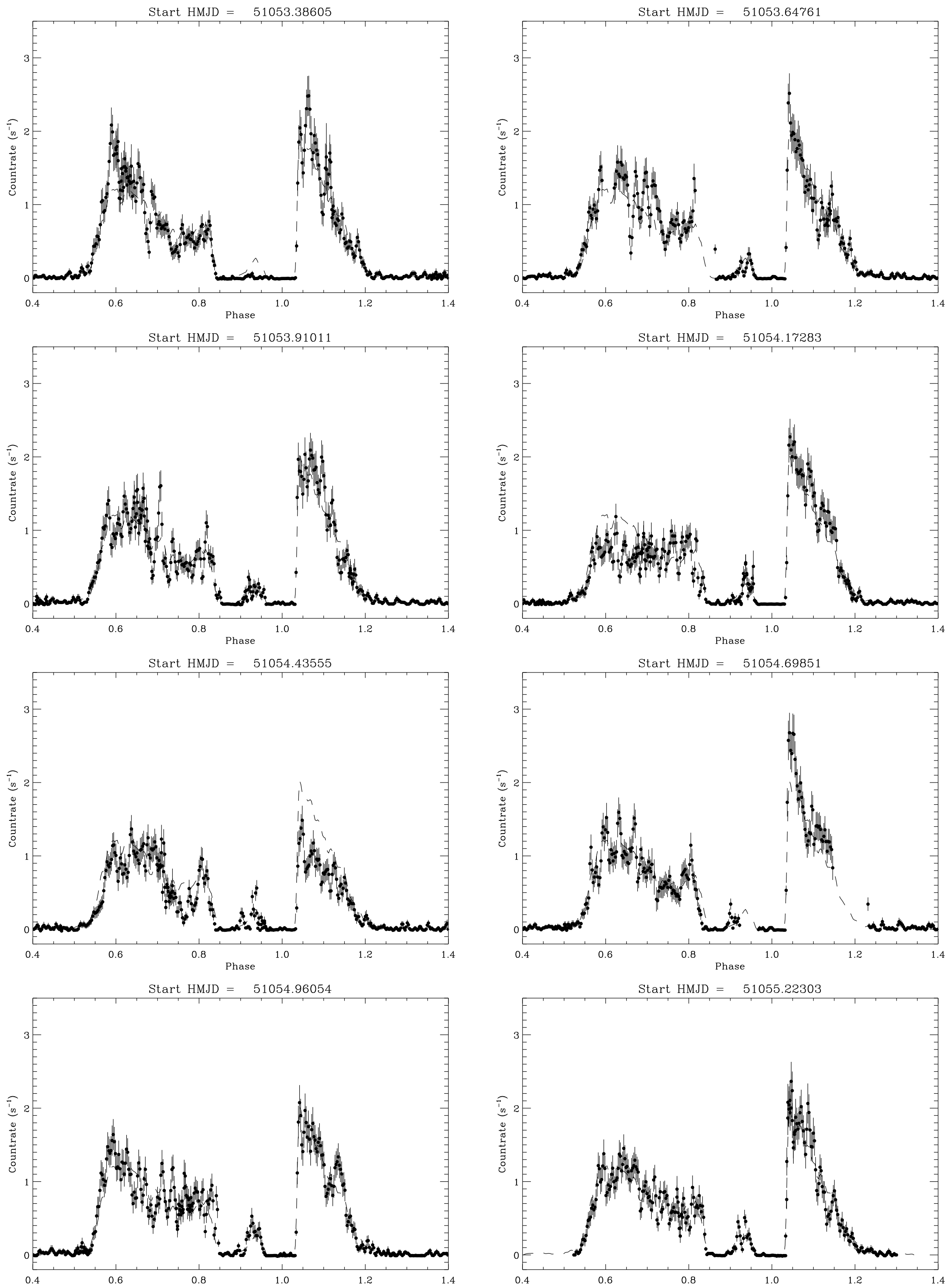
Start HMJD = 51053.38605
Start HMJD = 51053.64761
Start HMJD = 51053.91011
Start HMJD = 51054.17283
Start HMJD = 51054.43555
Start HMJD = 51054.69851
Start HMJD = 51054.96054
Start HMJD = 51055.22303
Countrate (s^{-1})
Phase
0
1
2
3
0.4
0.6
0.8
1.0
1.2
1.4

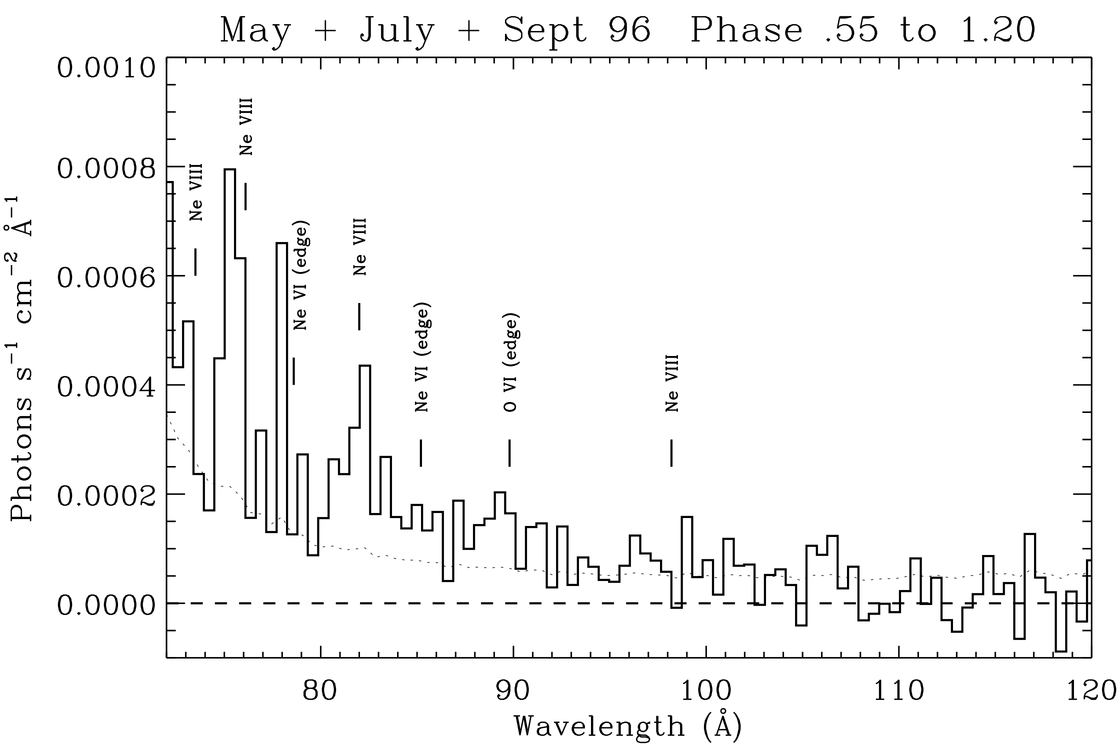
May + July + Sept 96 Phase .55 to 1.20
Photons s^{-1} cm^{-2} Å^{-1}
0.0010
0.0008
0.0006
0.0004
0.0002
0.0000
Ne VIII
Ne VIII
Ne VI (edge)
Ne VIII
Ne VI (edge)
O VI (edge)
Ne VIII
80
90
100
110
120
Wavelength (Å)

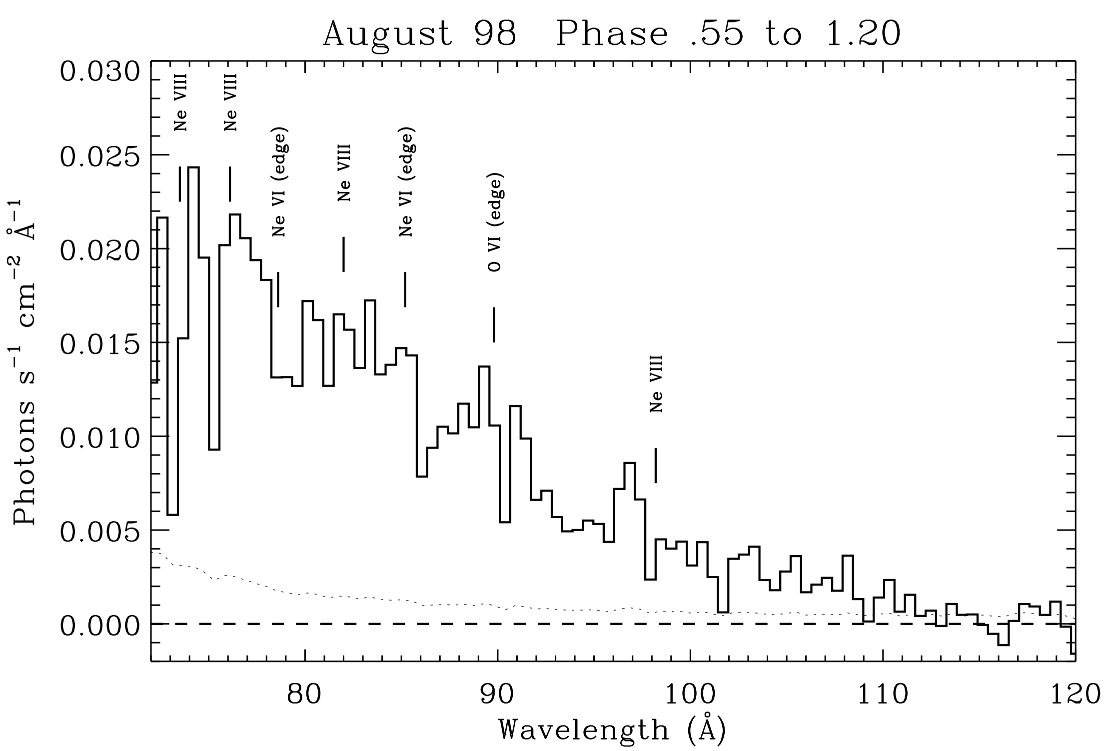
August 98 Phase .55 to 1.20
Photons s^{-1} cm^{-2} Å^{-1}
0.030
0.025
0.020
0.015
0.010
0.005
0.000
Ne VIII
Ne VIII
Ne VI (edge)
Ne VIII
Ne VI (edge)
O VI (edge)
Ne VIII
80
90
100
110
120
Wavelength (Å)

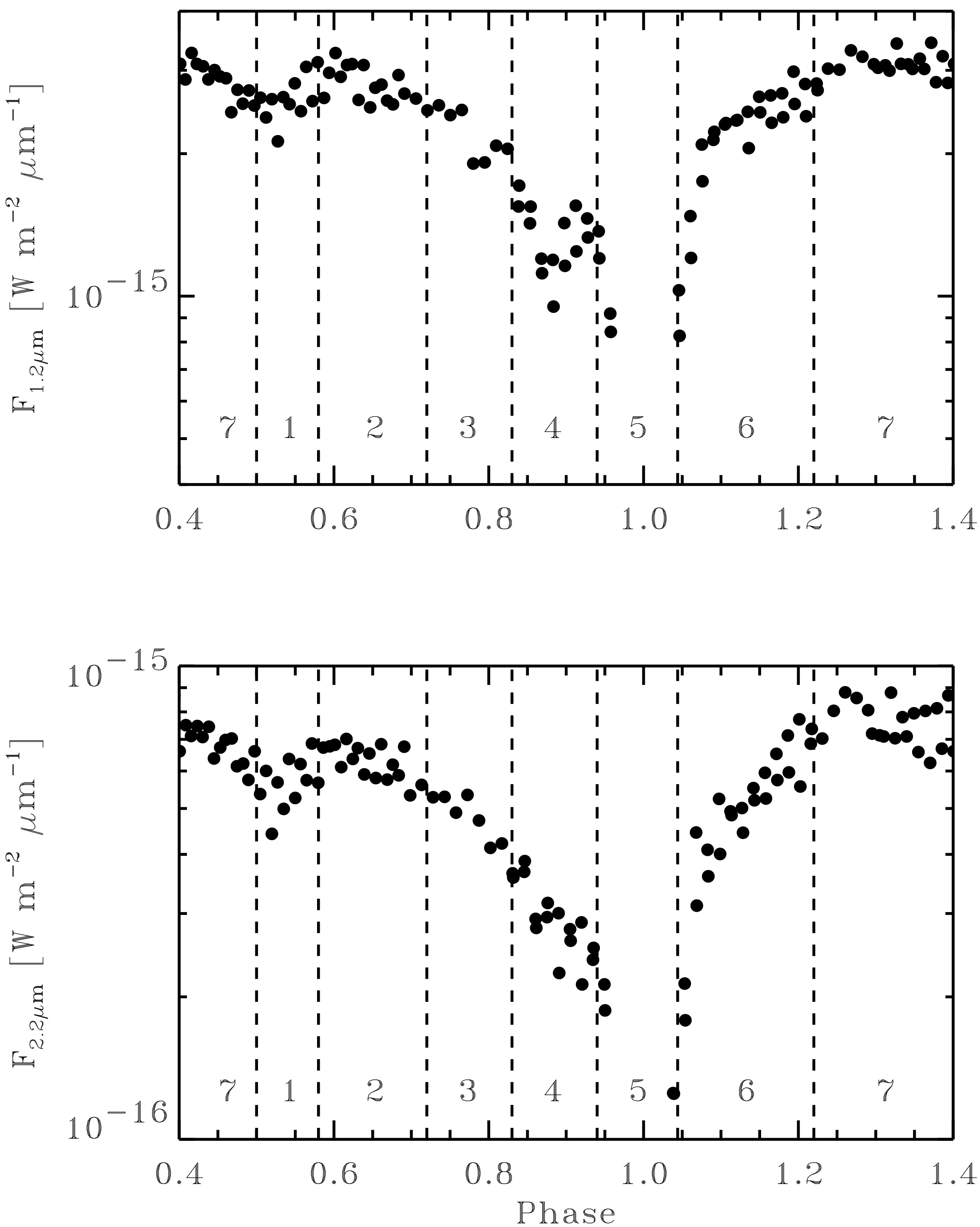

$F_{1.2\mu m}$ [W m^{-2} μm^{-1}]
10^{-15}
7
1
2
3
4
5
6
7
0.4
0.6
0.8
1.0
1.2
1.4
$F_{2.2\mu m}$ [W m^{-2} μm^{-1}]
10^{-15}
10^{-16}
7
1
2
3
4
5
6
7
0.4
0.6
0.8
1.0
1.2
1.4
Phase

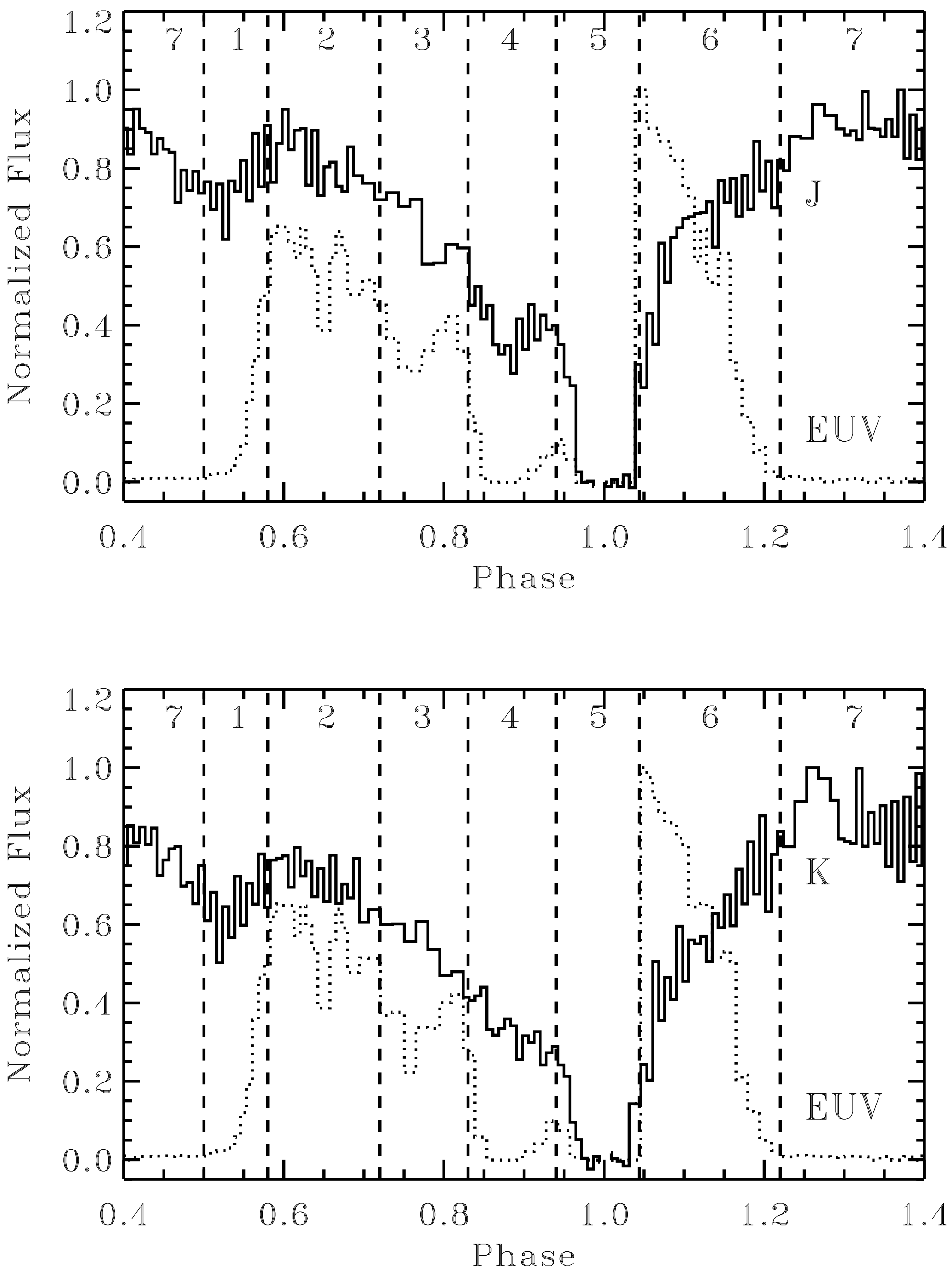
7
1
2
3
4
5
6
7
J
EUV
Normalized Flux
Phase
0.0
0.2
0.4
0.6
0.8
1.0
1.2
0.4
0.6
0.8
1.0
1.2
1.4
7
1
2
3
4
5
6
7
K
EUV
Normalized Flux
Phase

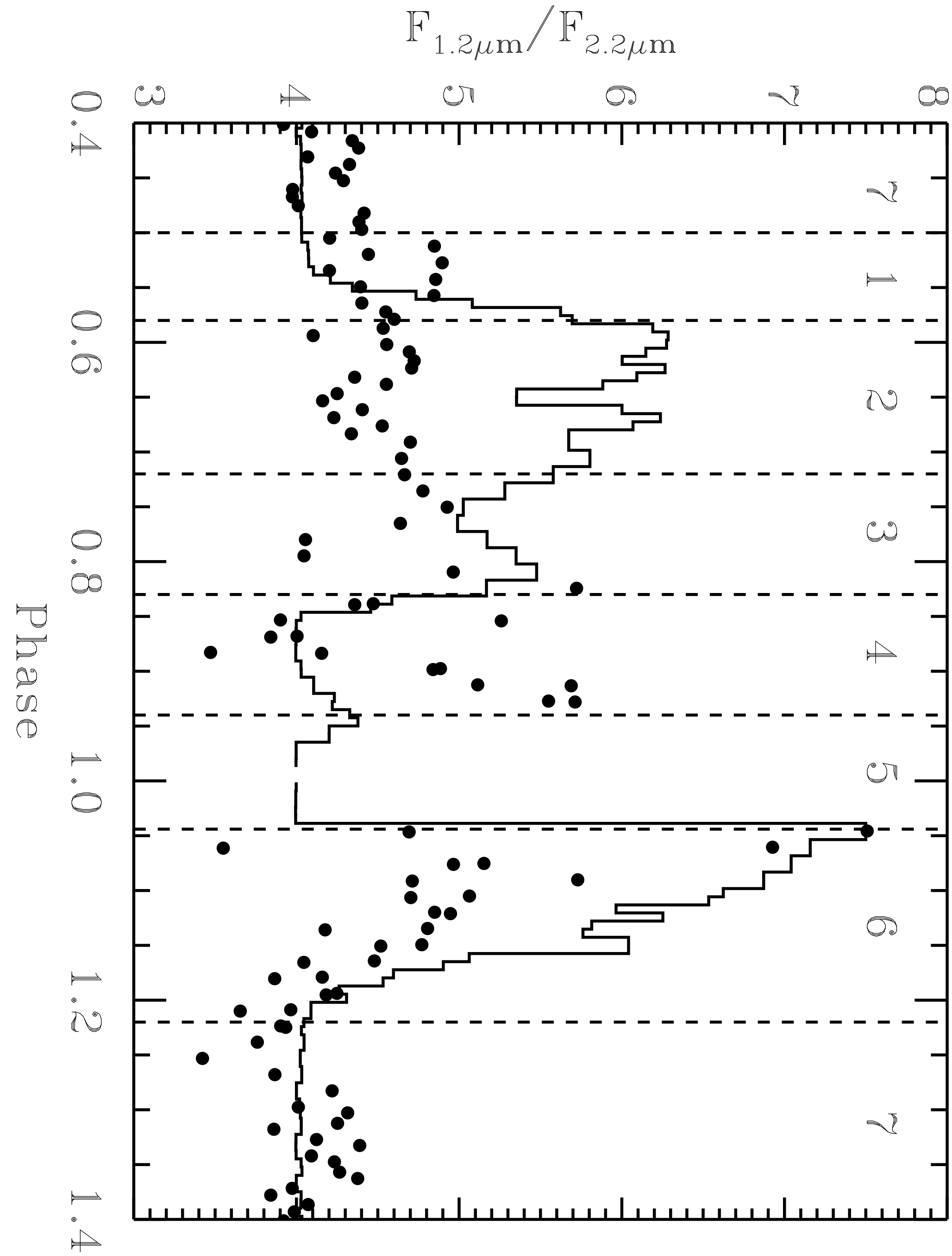
F1.2μm/F2.2μm
3
4
5
6
7
8
Phase
0.4
0.6
0.8
1.0
1.2
1.4
7
1
2
3
4
5
6
7